RSC Advances

ROYAL SOCIETY OF CHEMISTRY

www.rsc.org/advances

Journal Name

ARTICLE

Controlled synthesis of dual-emission hierarchical quantum dots hybrid nanostructure as robust ratiometric fluorescent sensor

Received 00th January 20xx,
Accepted 00th January 20xx

DOI: 10.1039/x0xx00000x

www.rsc.org/

Jing Wang,[a*] Chenxing Jiang,[a] Fang Yang,[b] Aimin Chen,[a] Ligeng Wang[a] and Jun Hu[a*]

Constructing robust dual/multi-emission fluorescence nanoparticle with tunable intensity ratios and colors is of particular interest in highly sensitive ratiometric probe development. Herein, we have fabricated a novel silica-coated dual-emission hierarchical hybrid nanostructure ($CdTe@SiO_2@CdTe@SiO_2$) with two sizes of CdTe quantum dots (QDs) spatially separated, which was composed of green-emitting QDs in situ grown onto the surface of silica nanoparticle embedded with red-emitting QDs. Both fluorescence intensity ratios and colors can be effectively adjusted by simple control of refluxing time or precursor concentrations of the outer QDs. This complex $CdTe@SiO_2@CdTe@SiO_2$ nanoparticle exhibited stronger photo and chemical stability as well as better biocompatibility than previously reported QDs-silica-QDs analogues. As a proof of principle, the dual-emission fluorescence silica nanohybrid was served as a reliable ratiometric probe to precisely monitor gold nanoparticle concentration through a fluorescence energy transfer mechanism.

Introduction

Ratiometric fluorescence technique for constructing various chemo/bio sensors has attracted considerable attention in last few years, benefiting from its merits in terms of improved sensitivity at trace quantity levels of analytes and self-referencing capability for environmental effects.[1-3] More importantly, the fluorescence signal variation of ratiometric probe accompanied with change of fluorescence color observed by naked eye is considered to be a conceivable way to point out the presence of an analyte.[4,5] Ratiometric fluorescence detection is mainly based upon dual-emission fluorescence nanoparticles (NPs), which are generally obtained by combining two different fluorophores in one nanoparticle, one fluorophore as the reference and another as a signal report unit.[6,7] In the past decades, fluorescence organic dyes[8-11] and semiconductor quantum dots (QDs)[12-18] have been well studied as luminescence elements for the fabrication of ratiometric sensing platforms. Compared with organic dyes, QDs display several exceptional advantages in many aspects, such as greater brightness, stronger stability with respect to photobleaching, narrower spectral line-width and size-controlled luminescence properties.[19] Most particularly, QDs with different sizes can be excited by a single wavelength and emit at different bands, affording the convenience of incorporating different-sized QDs and enabling the feasibility to create a multicolor system on the basis of a ratiometric fluorescence probe.[20]

Despite the rapid development of nanotechnology, the integration of different-sized QDs with well preserved emission properties has been a long standing challenge. Silica, a versatile and biocompatible material for both substrates and coating layers on nano-objects,[21,22] exhibits unique processibility that enabling facile incorporation of different fluorophores and a variable space between the inner reference and surface attached signal. Up to now, the common strategy for fabrication of QD-based dual-emission fluorescence NPs was electrostatic self-assembly or covalent immobilization of 'signal QDs' onto silica substrates embedded with the 'reference QDs'. Although these dual-emission hybrid silica NPs gained significant attention and have been broadly exploited for metallic ions,[15,23,24] gases,[25] and organic small molecules[13,26,27] sensing, high-quality QDs-based hybrid nanostructure remained elusive: Firstly, QD-embedded silica NPs prepared from Stöber method had poor monodispersity,[12,28] which can hardly serve as homogeneous substrates for surface NPs loading. Secondly, adopting the electrostatic self-assembly protocol,[13,29] the adsorbed QDs were unstable against external pH variations and easy to detach from the substrate, most especially the loading density was relatively low because of the interparticle electrostatic repulsion of similarly charged NPs. Thirdly, through covalent immobilization approach,[14,15] the coupling efficiency was

[a] College of Chemical Engineering, Zhejiang University of Technology, Hangzhou, 310014, P.R. China.
E-mail:Jinqw1986@zjut.edu.cn; hjzjut@zjut.edu.cn.
[b] School of Laboratory Medicine, Hubei University of Chinese Medicine, Huangjia Lake West Road, Wuhan, 430065, P.R. China.
† Footnotes relating to the title and/or authors should appear here.
Electronic Supplementary Information (ESI) available: [details of any supplementary information available should be included here]. See DOI: 10.1039/x0xx00000x

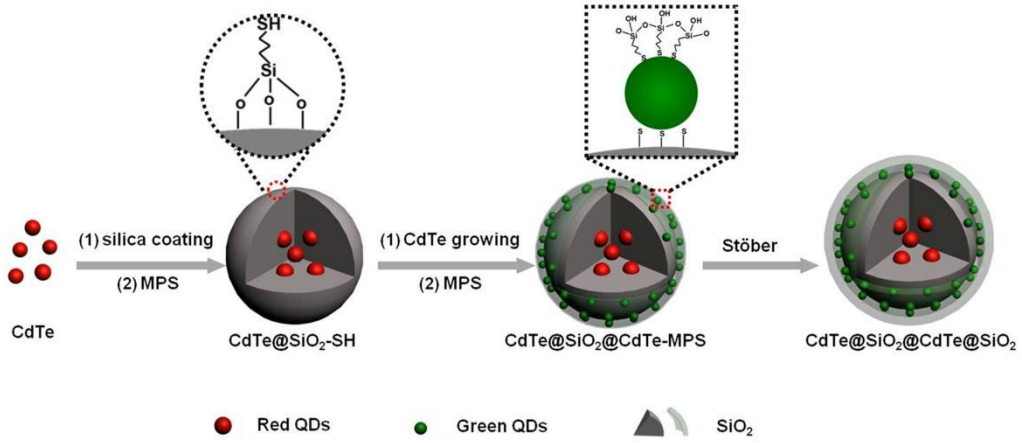

Scheme 1. Schematic illustration for the preparation of $CdTe@SiO_2@CdTe@SiO_2$ nanoparticles.

uncontrollable and the QDs emission intensity as well as fluorescence spectra (including peak position) tended to suffer a great destruction due to the damage of QD ligands protection. Finally, it should be noted that the practical bio-applications of these ratiometric probes were hindered by several problems such as photo and chemical instability in harsh environments and cytotoxicity caused by the release of heavy metal ions from the outer unprotected QDs.[30,31] With these insights, it is essential to develop an alternative dual-emission fluorescence nanoparticle with high fluorescence efficiency, tunable fluorescence intensity ratios and colors as well as excellent stability and biocompatibility that could be applied to visual identification of targets in complex biological samples.

In this contribution, we developed highly stable QDs incorporated dual-emission hierarchical fluorescent silica NPs ($CdTe@SiO_2@CdTe@SiO_2$ NPs) for ratiometric sensing applications. As illustrated in **Scheme 1**, the red-emitting CdTe QDs embedded silica spheres with thiolated surface were employed as hybrid templates, for in situ growing of green-emitting CdTe QDs, achieving both tunable fluorescence intensity ratios and color changes. These $CdTe@SiO_2@CdTe$ NPs were subsequently encapsulated with another silica layer to provide robust photo-chemical stability and biocompatibility. The time- and concentration controlled synthetic strategy for dual-emission silica NPs with desired fluorescence intensity ratios and colors was established, and the building-up process was studied in detail. The advantages of current $CdTe@SiO_2@CdTe@SiO_2$ NPs, against previously reported ratiometric probes, in terms of stability and cytotoxicity were also demonstrated. Finally, a fluorescence energy transfer system between $CdTe@SiO_2@CdTe@SiO_2$ NPs and gold nanoparticle (AuNPs) has been proposed to illustrate the practicability of the newly prepared ratiometric fluorescence NPs.

Experimental section

Synthesis of $CdTe@SiO_2$ Composite NPs Modified by Thiol and Amino Groups.

Thiol-capped $CdTe@SiO_2$ (QS-SH) core-shell structured fluorescent silica nanospheres were synthesized by a modified reverse microemulsion method.[32,33] Briefly, sodium hydroxide (NaOH, 16 μL, 1M) and ammonium hydroxide ($NH_3 \cdot H_2O$, 18 μL, 25 wt%) were added into 1 mL of red-emitting QD (5×10^{-6} M) solution, and incubated for 40 min. Then, the above solution and tetraethyl orthosilicate (TEOS, 100 μL) were introduced into a system containing cyclohexane (15 mL), n-hexanol (1.5 mL), Triton X-100 (2.25 mL) and poly(diallyldimethylammonium chloride) (PDDA, 20 μL, 12.8 mM). Another $NH_3 \cdot H_2O$ (60 μL, 25 wt%) was introduced into the mixture after stirring for 30 min. Subsequently, the reaction system was sealed and stirred for three days. Afterwards, 3-mercaptopropyl-trimethoxysilane (MPS) (8 μL) was added, and the reaction system was stirred for another 24 h. To obtain amino-functionalized $CdTe@SiO_2$ nanoparticles ($QS\text{-}NH_2$),[34] ten microliter of 3-aminopropyltriethoxysilane (APTES) were added to the microemulsion system instead of MPS, and stirred for another 12 h. The reaction was terminated by adding isopropanol (20 mL). The precipitates were collected by centrifugation and washed by isopropanol, ethanol and water in sequence, then dispersed in deionized water for future use.

Synthesis of MPS Modified Dual-Emission $CdTe@SiO_2@CdTe$ NPs.

The outer green fluorescent QDs layer was constructed via in situ growth method.[35] Typically, the as-prepared QS-SH solution (40 mL) (originated from 0.5 mL of TEOS), cadmium chloride ($CdCl_2$, 0.04 M, 4 mL) and trisodium citrate dihydrate (400 mg) was added into a three-necked flask and stirred for 1 h at room temperature. After that, sodium tellurite (Na_2TeO_3, 0.01 M, 4 mL), mercaptosuccinic acid (MSA, 50 mg) and sodium borohydride ($NaBH_4$, 50 mg) were added under vigorous stirring. Then the mixture was refluxed at 100 °C under N_2 flow. MPS (50 μL) was introduced when the fluorescence of the mixture turned to green (25 min), and the resultant reaction system was refluxed for another 5 min. The obtained MPS modified $CdTe@SiO_2@CdTe$ (QSQ-MPS) NPs was centrifuged and washed with deionized water for three times. For the preparation of time-driven QSQ-MPS NPs, the mixture was refluxed at 100 °C for 0, 5, 12, 14, 15, 16, 17, 19,

21, and 25 min respectively and incubated with MPS. For the preparation of concentration-driven QSQ-MPS NPs, the mixture containing half concentration of the same precursors was refluxed at 100 °C for 25 min and incubated with MPS.

Synthesis of Dual-Emission CdTe@SiO_2@CdTe@SiO_2 NPs.

CdTe@SiO_2@CdTe@SiO_2 (QSQS) hierarchical hybrid NPs were prepared with a revised Stöber method.[36] Typically, the QSQ-MPS NPs was first redispersed in ethanol (5 mL). The above solution was mixed with $NH_3 \cdot H_2O$ (75 μL) and deionized water (150 μL). Then, each 12.5 μL of TEOS was injected and stirred for 1.5 h until the desired shell thickness was reached. The QSQS NPs with TEOS feeding amount of 12.5 and 50 μL were collected by centrifugation and washed with ethanol and deionized water for several times.

Stability Measurements.

To evaluate the chemical stability, the QSQS, QSQ1, and QSQ2 NPs (the preparation of QSQ1 and QSQ2 NPs was shown in **Supporting Information**, 0.2 mg mL^{-1}) were redispersed in solutions with different pH value (3, 4, 5, 6, 7, 7.4, 8, 9, and 10; the pH value of the solutions were adjusted using phosphate buffer), respectively. Thirty minutes later, the fluorescence intensity spectra were recorded, and the intensity ratios (I_{520}/I_{670}) of each spectrum were calculated. To measure the long-term colloidal stability, the QSQS, QSQ1, and QSQ2 NPs (0.5 mg mL^{-1}) were incubated in water and phosphate buffer solutions (PBS, with the pH of 3, 6, 7.4, and 9), and the digital photographs were captured after 24 h. To measure the photostability, the QSQS, QSQ1, and QSQ2 NPs (0.2 mg mL^{-1}) in water were excited continuously for 1 h with a 450 W xenon lamp and the fluorescence intensity ratios were recorded. To evaluate the stability against various metal ions, 100 μL of QSQS, QSQ1, and QSQ2 NP solutions (2 mg mL^{-1}) and a series of selected metal ions (K^+, Fe^{3+}, Ba^{2+}, Zn^{2+}, Cd^{2+}, Mg^{2+}, Ca^{2+}, Co^{2+}, Ni^{2+}, Ag^+, Cu^{2+}, Hg^{2+}; 10 μM) were mixed in 1.0 mL of PBS (10 mM, pH 7.4), respectively. After 30 minutes, the mixtures were then added into a spectrophotometer quartz cuvette, and the spectra were measured under the excitation of 380 nm.

Cytotoxicity Measurements.

For MTT assay, cells were cultured in 96 well plates and then were incubated up to about 16 h and grown to about 80% confluence before experiments. QSQS NPs dispersed in DMEM and different concentrations were added to each well to achieve a final concentration. Cells were then incubated in these medium containing QSQS NPs at 37 °C and in 5% CO_2 atmosphere for 24 h. After incubation, all cells were washed with PBS to remove excess QSQS NPs and placed in fresh solutions 200 μL before next experiments. At the end of the incubation, 20 μL stock MTT (5 mg mL^{-1}) was added to each well, and cells were then incubated for 4 h at 37 °C. The supernatant was abandoned, and 150 μL of DMSO per well was added to dissolve the produced formazan and the plates were shaken for an additional 10 min, and the absorbance of the purple formazan was recorded on Enzyme-linked immunosorbent detector at 490 nm. The MTT assays for QSQ1 and QSQ2 NPs were carried out with the same procedure as the QSQS NPs.

Ratiometric Detection Based on Fluorescence Energy Transfer.

Before detection, QSQS NPs with the silica shell thickness of 2 nm were functionalized with amino groups (termed as QSQS-NH_2).[37] Briefly, the QSQS NPs were diluted to 2 mL with ethanol followed by the addition of 200 μL APTES. After being vigorously stirred for 5 h, the mixture was centrifuged, washed with water and ethanol several times, to remove excess reactants. A fluorescence energy transfer system was employed for ratiometric fluorescence detection. To a 2 mL calibrated test tube 100 μL of the ratiometric probe solution (2 mg mL^{-1}) and certain amounts of AuNPs were sequentially added. The mixture was then diluted to a final volume of 1.0 mL with 0.01 M PBS (pH 7.4) and mixed thoroughly. Two minutes later, the mixture was transferred to a 3 mL cuvette and the fluorescence intensity of solution was recorded with the excitation wavelength of 380 nm.

Results and discussion

The fabrication flow of the proposed, robust and eco-friendly, silica-coated QD-embedded dual-emission hierarchical hybrid silica NPs is illustrated in **Scheme 1**. The synthesis started from the red-emitting MPA-capped CdTe QDs, which were fully wrapped by a silica shell to get QD-embedded silica (QS) NPs. The composite QS NPs were functionalized with thiol group (QS-SH), followed by in situ growing with green-emitting CdTe QDs (QSQ) under refluxing. Then, they were incubated with MPS (QSQ-MPS) and encapsulated by another silica shell (QSQS) to provide stability and biocompatibility.

Monodisperse CdTe QDs with an average diameter of 4.3 ± 0.3 nm (**Fig. 1A**) were prepared by a one-pot process. Multicore-shell QS NPs were obtained through a modified reverse microemulsion method. In order to retain the initial fluorescence properties of QDs, the red-emitting CdTe QDs was first incubated with a mixture composed of NaOH and $NH_3 \cdot H_2O$ solution. Transmission electron microscopy (TEM)

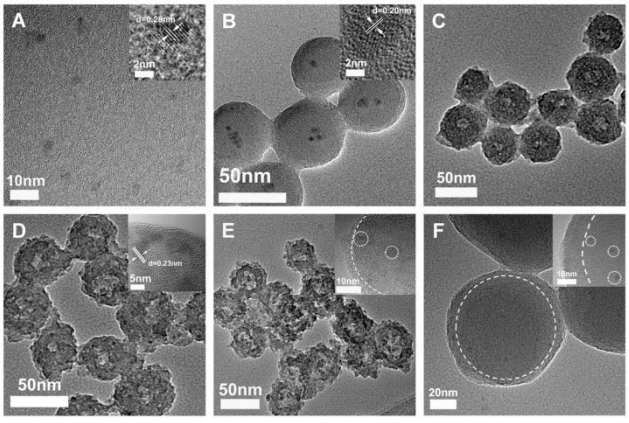

Fig. 1. TEM images of CdTe (A), QS (B), QS-SH (C), QSQ-MPS (D), and QSQS NPs with TEOS feeding amount of 12.5 (E) and 50 μL (F), respectively. Insets are the corresponding HRTEM images.

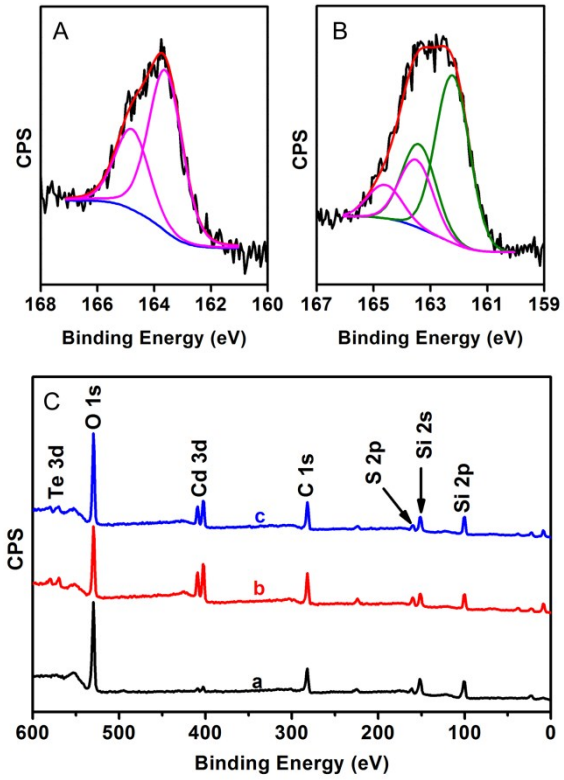

Fig. 2. XPS spectra of S 2p signals in QS-SH (A), and QSQ-MPS (B) NPs. XPS overview spectra (C) of QS-SH (curve a), QSQ-MPS (curve b), and QSQS (curve c) NPs.

image presented that the QDs were fully encapsulated and the as-synthesized QS NPs were well-dispersed with an average size of 42.7 ± 6.7 nm (**Fig. 1B** and **Fig. S1A**). It could also be observed that the d-spacing of adjacent fringes (Inset of **Fig. 1A, B**) for the CdTe and QS NPs were 0.28 and 0.20 nm, which were in agreement with the (100) and (101) plane spacing of CdTe structures, respectively. Noticeably, there were multiple CdTe QDs encapsulated into silica spheres, probably owing to the addition of PDDA as polyelectrolyte.[32] The fluorescence quantum yield (QY) of CdTe QDs encapsulated in silica particles reached 29%. Compared with QS NPs prepared by Stöber method, this complex NPs possessed highly uniform spherical morphology, affording a desirable substrate for surface NPs loading. The silica surface of QS NPs were subsequently grafted with thiol groups using MPS as organosilane coupling agent, which possess strong chemical affinity to the metal atoms of QDs. The existence of the surface −SH groups was confirmed by the XPS analysis. In the overview spectrum (**Fig. 2C**, curve a), the binding energies of O 1s, S 2p, Si 2s, and Si 2p were found to be 532.6, 163.6, 154.6, and 103.6 eV, respectively. The binding energy profile of S 2p was shown in **Fig. 2A**. The spectrum was fitted by two peaks located at 163.6 and 164.8 eV, attributed to S $2p_{3/2}$ and S $2p_{1/2}$.[38] Specially, the hydrolyzed organosilane was visualized as a corona surrounding the surface of QS NPs (**Fig. 1C**), suggesting the successful attachment of this organosilica layer around QS NPs surfaces. The outer green fluorescent CdTe QDs were in suit grown on the thiolated surface using MSA as a costabilizer. This step was first characterized with XPS. As shown in **Fig. 2C**, compared with the original QS-SH (curve a), the emergence of new Cd 3d and Te 3d peaks in the QSQ-MPS NPs (curve b) were ascribed to that of CdTe QDs reported elsewhere.[39] Furthermore, the binding energy of S 2p peak of the QS-SH NPs at 163.7 eV was observed (**Fig. 2A**) while this peak was shifted to 162.8 eV for the QSQ-MPS NPs (**Fig. 2B**). Through the deconvolution of corresponding peak, the new S 2p binding energy could be attributed to the sulfur from the Cd-S– bond in CdTe QDs.[40] High-resolution TEM analysis revealed that the CdTe QDs can be also clearly seen to immobilize on the surface of silica NPs pre-coated with MPS (**Fig. 1D**). The inset showed an interplanar spacing of 0.23 nm, corresponding to the lattice of CdTe QDs and indicating that CdTe QDs were well-crystallized. The average size of QSQ-MPS NPs slightly increased to 47.5 ± 7.2 nm (**Fig. S1B**). In order to retain the green fluorescence of CdTe QDs and improve their stability, another silica layer was homogeneously deposited. Here we demonstrated the seeded growth of the QSQ-MPS in an ethanol/water mixture using TEOS as the silica source. **Fig. 1E** shows that the average size of QSQS NPs was 51.9 ± 6.0 nm, indicating that the thickness of the silica layer was ~2 nm. This existence of silica shell was further confirmed by XPS analysis. As demonstrated in **Fig. 2C** and **Table S1**, silica coating on QSQ-MPS resulted in an increase in the relative elemental compositions of oxygen and silicon and a decrease in the unrelative elemental compositions of sulfur, cadmium, and tellurium. The fluorescence QY of green-emitting CdTe QDs in QSQS NPs was about 43%. The thickness of this silica shell can be controlled by the well-known Stöber process. As illustrated in **Fig. 1F** and **Fig. S1D**, when TEOS feeding amount turned to 50 µL, monodispersed core–shell NPs with a smoother surface and an increased shell thickness of 20 nm were successfully synthesized.

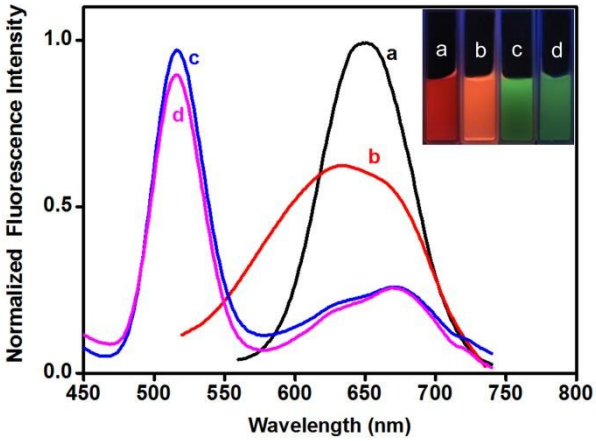

Fig. 3. Fluorescence emission spectra (λex=380 nm) of CdTe (a), QS-SH (b), QSQ-MPS (c), and QSQS (d) NPs. The inset photos show the corresponding fluorescence colors under a 365 nm UV lamp, respectively.

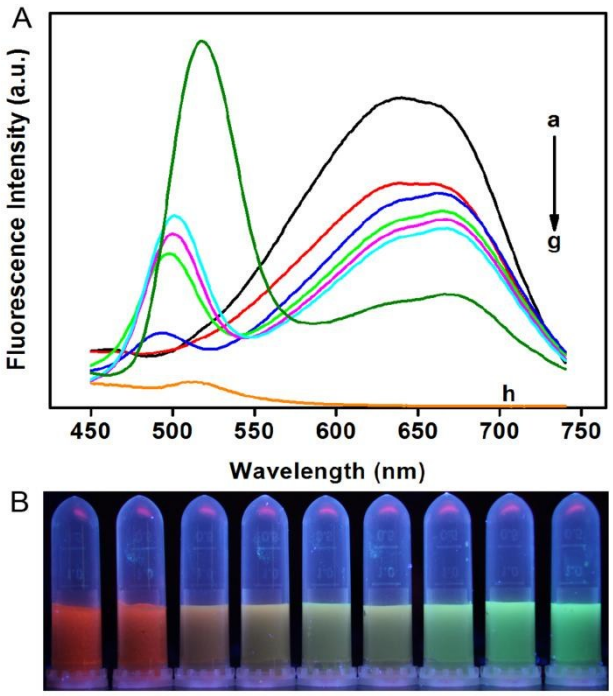

Fig. 4. (A) Fluorescence emission spectra (λ_{ex}=380 nm) of the resultant QSQ NPs at different steps including QS-SH (a), after adding $NaBH_4$ (b), heating to 100 °C (c), refluxing at 100 °C for 10 (d), 20 (e), 30 (f) min, and after adding MPS (g), respectively. Curve h shows the fluorescence spectra of corresponding supernatant after adding MPS. (B) Fluorescence colors of the QSQ-MPS NPs refluxed at 100 °C for 0, 5, 12, 14, 15, 16, 17, 19, 21, and 25 min, respectively.

The fluorescence spectra of CdTe, QS-SH, QS-MPS, and QSQS NPs are shown in **Fig. 3**. The original CdTe QDs displayed a fluorescence maximum at 650 nm (curve a) and exhibited a strong red fluorescence under a UV lamp (a of inset). After silica coating and MPS modification, the fluorescence intensity of QS-SH NPs was decreased and the characteristic peak was located at 640 nm. The slight blue-shift of emission peak was probably due to the confinement of CdTe inside the silica cavity with less polarity compared to bulk solution.[41,42] The orange red fluorescence (b of inset) was captured under a UV lamp, further revealing the blue-shift phenomenon. When the green-emitting QDs were grown onto the surface of the QS-SH NPs, the fluorescence spectrum (curve c) of the resultant NPs presented two characteristic peaks of the inner (670 nm) and outer (520 nm) QDs, respectively. However, it should be noted that there was a large red-shift (20 nm) of the emission from red-emitting QDs, which can be explained by the possible ripening of these nanocrystals under further refluxing conditions. To clarify this assumption, we conducted additional controlled experiments. As illustrated in **Fig. S2**, the fluorescence emission peaks of the QS-SH, QS-SH+$CdCl_2$, QS-SH+MSA, and QS-SH+$CdCl_2$+MSA solutions refluxed under the same conditions were almost consistent with that of QSQ-MPS NPs, which indicated that the red-shift was not due to the growth of outer QDs but the further growth of the inner ones. After silica coating, the peaks of dual-emission bands remain unchanged and 95% of the initial fluorescence of the outer QDs was preserved. The corresponding fluorescence colors of QSQ-MPS and QSQS NPs were also recorded (c and d of inset) for a direct comparison with those of the red-emitting CdTe and QS-SH NPs. Visibly, there was a significant change of fluorescence color under a UV lamp. The result suggested that the green-emitting QDs were successfully in suit grown onto the surface of the red QD-embedded silica NPs and both were photoluminescent under a single excitation.

To understand the growth evolution of the outer QDs, we studied the fluorescence spectra step by step. As displayed in **Fig. 4A** before heating there was no emission peak at short wavelength (curve a, b), while the green fluorescence peak was apparent after heating (curve c) and became stronger and stronger with the increase of refluxing time (curve d, e, and f). This tendency was consistent with the formation of individual CdTe QDs in other report.[43] With the introduction of MPS, the fluorescence intensity increased almost one-fold and the emission peak red-shifted to 520 nm (curve g). During the fabrication procedure, it is critical to pre-coat QSQ NPs with MPS for two important reasons. 1) Clearly, both the silica surface and solution allows for the growth of CdTe QDs, MPS can gather the QDs which were dispersed individually in the solution onto the surface of silica,[44] producing more QDs on the particle, resulting in the decreased amounts of QDs in corresponding supernatant (curve h), and consequently the improvement of green fluorescence of QSQ NPs. The red-shift of the fluorescence peak after adding MPS may be attributed to interparticle plasmon coupling caused by nanoparticle clustering.[45] 2) The other is the direct incubation of QSQ NPs with MPS under refluxing conditions, which directs MPS to pre-coat and protect CdTe QDs and induces the subsequent homogeneous silica coating.[38] In the preparation of dual-emission fluorescence NPs, the tunable fluorescence intensity ratios and colors were more popular. QSQ-MPS NPs with various fluorescence intensity ratios and colors can be readily obtained through accurate adjustment of the reaction time (0-25 min). The typical fluorescence photograph of as-prepared QSQ-MPS NPs is presented in **Fig. 4B**. The superior tunability of the fluorescence colors over the very-broad spectral range is important for the use of the dual-emission NPs as the ratiometric probes in highly sensitive detecting for background-interference biological medium.[6] Moreover, the adjustable fluorescence properties can be fulfilled by concentration-driven strategy. As depicted in **Fig. S3**, by feeding half amounts of precursors, the green fluorescence of dual-emission QSQ-MPS NPs converted to yellow fluorescence under the same refluxing time.

For the dual-emission hybrid NPs to be used as a ratiometric probe, stability is a crucial factor to be considered. The pH buffering systems were optimized by monitoring the fluorescence chemical stability of QSQS, QSQ1, and QSQ2 NPs in PBS. As shown in **Fig. 5A**, the fluorescence intensity ratios (I_{520}/I_{670}) of QSQ1 and QSQ2 NPs were strongly influenced by minor variations in the range of pH values from 3.0 to 7.0 due to the green fluorescence decrease of the outer QDs under acidic conditions, indicating poor chemical stability. In contrast, QSQS NPs remained stable in a wide pH range of 3−10. The long-term colloidal stability of corresponding NPs against

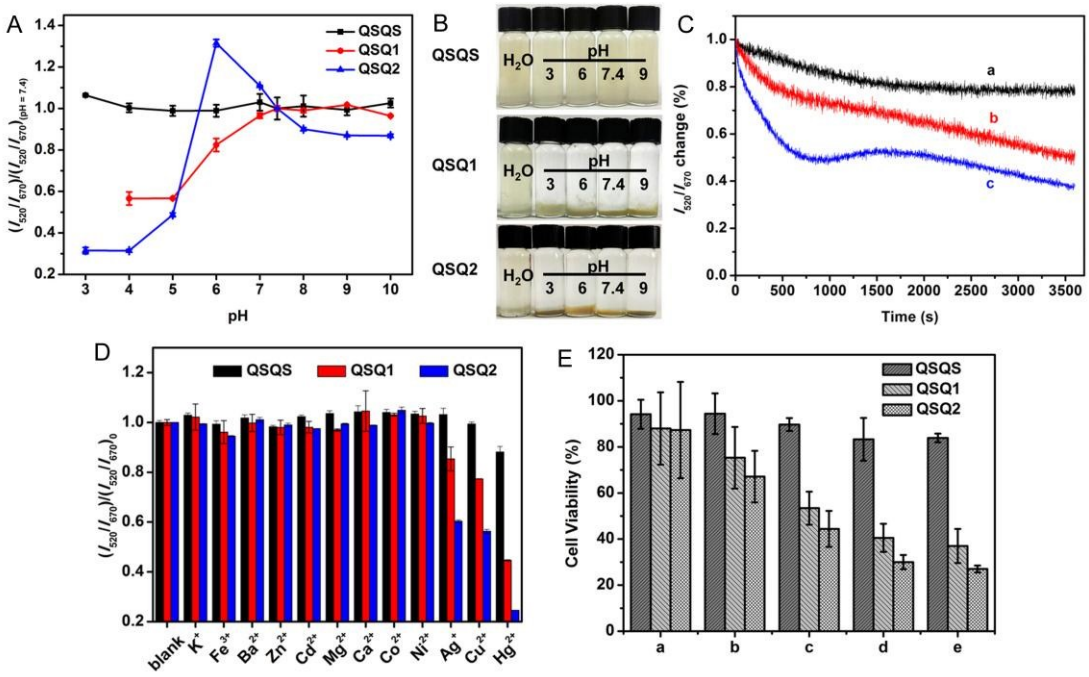

Fig. 5. (A) pH dependent response of the QSQS, QSQ1 and QSQ2 (0.2 mg mL^{-1}) ratiometric fluorescence NPs. (B) Digital photographs of the QSQS, QSQ1 and QSQ2 (0.5 mg mL^{-1}) NPs disepered in water and PBS for 24 h. (C) Time-dependent fluorescence intensity ratio (λ_{ex}=380 nm) of QSQS (a), QSQ1 (b), and QSQ2 (c) NPs. (D) Changes of fluorescence intensity ratios (I_{520}/I_{670}) of the QSQS, QSQ1 and QSQ2 (0.2 mg mL^{-1}) NPs in the presence of various metal ions (10 μM) in the PBS (pH 7.4, 10 mM). (E) Cytotoxicity of QSQS, QSQ1, and QSQ2 NPs with different concentrations and incubation for 24 h with HeLa cells, (a) 5, (b) 50, (c) 100, (d) 500, (e) 1000 (μg mL^{-1}).

water and PBS (pH 3, 6, 7.4, and 9) was also monitored (**Fig. 5B**). As expected, QSQ1 and QSQ2 NPs were aggregated between pH 3-9 except the QSQS. At low pH values, the ligands were protonated while the ligands gradually detached from the surface of QDs under basic conditions, resulting in no longer conferring to colloidal stability to the NPs.[46] Nevertheless, towards QSQS NPs, the coated silica shell shielded the outer QDs against aggregation under harsh pH conditions. Also, the QSQS NPs had a higher tolerance to slat than QSQ1 and QSQ2 NPs. Besides chemical stability, the photostability of QSQS NPs was also investigated. **Fig. 5C** shows that the fluorescence intensity ratio (I_{520}/I_{670}) of QSQ2 NPs dropped to 37% of the original value in 1 h. Similarly, the fluorescence intensity ratio of QSQ1 NPs was also unstable under UV irradiation retaining only >50% of the original intensity ratio after irradiation for 1 h. Oppositely, the fluorescence intensity ratio of QSQS NPs was remarkably stable and decreased slightly under the same conditions, indicating the highest photostability (> 80%). The tolerance of the ratiometric probe against various metal ions (10 μM) was also examined by monitoring the fluorescence intensity ratio upon the addition of the nitrate salts (**Fig. 5D**). The results suggested that the presence of some heavy metal ions, such as silver, copper, and mercury had great effect on the fluorescence intensity ratio of the QSQ1 and QSQ2 NPs, which was consistent with previous studies.[14,15] However, there was no obvious change for QSQS NPs at similar concentrations. These results indicated the level of metal ions interference was inherently low for such QSQS NPs. Furthermore, the cytotoxicity of QSQS, QSQ1, and QSQ2 NPs was elaborately studied with MTT viability assay. As displayed in **Fig. 5E**, the cell lines maintained greater than 80% cell viability after 24 h of treatment with QSQS NPs at concentrations range from 5 μg mL^{-1} to 1 mg mL^{-1}, while the cell viability incubated with QSQ1 and QSQ2 NPs dropped to around 50% at the concentration of 100 μg mL^{-1}, and became negligible after addition 1 mg mL^{-1} of NPs. This can be ascribed to the low toxicity of the shell. The silica shell greatly protects the outer QDs from photobleaching,[47] while the silica layer has less susceptibility to oxidation than the bare QDs.[30] Since the release of Cd^{2+} could be avoided, QSQS prepared by this approach are more favorable for bio-applications.

We then studied energy transfer effect on the ratiometric signal readout. AuNPs were chosen as energy acceptors for exploring the energy transfer effect due to their large extinction coefficient and easy surface functionalization.[48] As negatively charged AuNPs (**Fig. S4**) and positively charged QSQS-NH_2 NPs mixed with each other, hybrid AuNP-QSQS assembly was formed by electrostatic attraction (**Fig. S5**). As a result, the emission band from outer QDs was remarkably quenched; in contrast, the red emission of inner QDs was only quenched to about one-fourth at the same conditions (**Fig. 6A**). It was easy to understand the smaller quenching effect of inner QDs than that of outer QDs. First, the separation distance of AuNPs to the outer QDs was rather small (<10 nm), while the distance between the inner QDs and AuNPs was large (>20 nm). Therefore, the fluorescence of inner QDs may be quenched via a surface energy transfer mechanism, instead

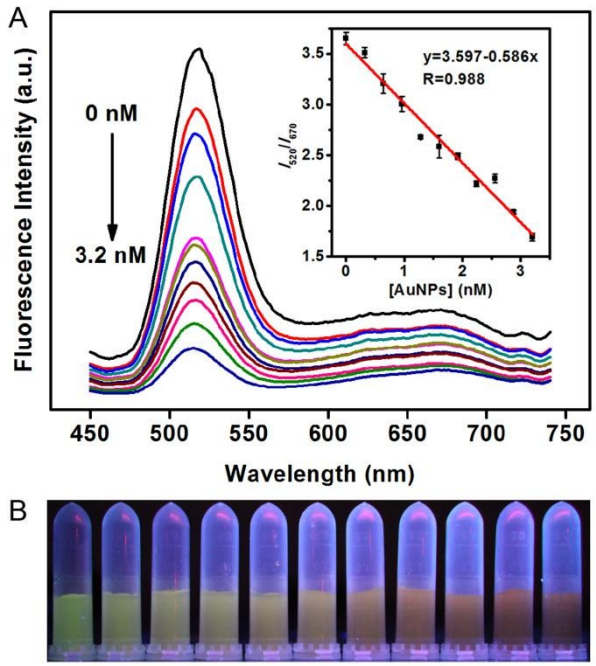

Fig. 6. (A) Fluorescence spectra (λ_{ex}=380 nm) of QSQS ratiometric fluorescence probe in the presence of various concentrations of AuNPs. The concentration of AuNPs from the top to the bottom: 0, 0.32, 0.64, 0.96, 1.28, 1.60, 1.92, 2.24, 2.56, 2.88, and 3.20 nM, respectively. The final concentration of the ratiometric probe was 0.2 mg mL^{-1}. Inset: linear fitting curve of I_{520}/I_{670} versus different concentrations of AuNPs. (B) Corresponding fluorescence photographs were taken under a 365 nm UV lamp.

of a resonance energy transfer mechanism as the outer QDs.[49,50] Second, the emission band of outer QDs completely overlapped with the AuNP absorption, while the red-emission of inner QDs was only partly overlapped (**Fig. S6**). Accordingly, the former was more significantly quenched due to higher energy transfer efficiency. To further verify the energy transfer phenomenon, the time domain spectroscopy was examined. As shown in Fig. S7, the decays of all the samples can be well fitted to a biexponential model. For the maximum emission of 520 nm, the average fluorescence lifetime of isolated QSQS NPs was 14.6 ns. After addition of AuNPs, the average fluorescence lifetime was decreased to 13.3 and 11.9 ns with the AuNPs concentration of 1.28 and 2.56 nM, respectively. Nevertheless, the fluorescence lifetime of the inner QDs was almost unchanged because of the low fluorescence intensity and the long distance barrier between donor and acceptor. The results indicated that the fluorescence energy transfer was happened from QSQS NPs to AuNPs and the outer QDs had higher energy transfer efficiency than the inner QDs. Because of strong wavelength dependent quenching, the ratios of I_{520}/I_{670} were decreased gradually with the increasing of concentration of AuNPs ranging from 0.0 to 3.20 nM, which can be used for the quantification of AuNPs with a correlation coefficient of 0.988, and the detection limit can be as low as 0.28 nM based on the definition of three times the deviation of the blank signal (3σ). Meanwhile, the visual detection of AuNPs by the naked eye under a UV lamp was feasible (**Fig. 6B**). Most importantly, both QSQS and AuNP surface can be functionalized by via well-established chemical modification,[51,52] such a QSQS-AuNP hybrid system is promising to achieve various ratiometric sensing especially for complex biological targets.

Conclusions

In summary, we have developed a versatile protocol for the synthesis of highly stable and biocompatible CdTe@SiO_2@CdTe@SiO_2 dual-emission hierarchical hybrid nanostructure with tunable fluorescence intensity ratios and colors. The as-prepared CdTe@SiO_2@CdTe@SiO_2 NPs displayed a higher fluorescence stability and lower cytotoxicity in comparison with their QDs-silica-QDs analogues. The in situ growth method combined with MPS-assisted silanization was critical to achieving a desired fluorescence intensity ratios and a homogeneous silica coating around the QD assemblies. Taking these advantageous properties, we have demonstrated the utility for visual detection of AuNPs concentration in aqueous solution based on energy transfer mechanism. Undoubtfully, the present contribution will enable us to make full use of high quality dual-emission NPs to build practical and reliable ratiometric sensing platforms.

Acknowledgements

We thank Prof. C. Zhang, from the Zhejiang University of Technology, Hangzhou, for the fluorescence experiments and gratefully acknowledge the financial support from National Natural Science Foundation of China (21405139, 31401510), the Scientific Research Start-up Funding of Zhejiang University of Technology (101010629).

Notes and references

1 X. Zhang, Y. Xiao and X. Qian, *Angew. Chem., Int. Ed.*, 2008, **47**, 8025-8029.
2 L. Y. Niu, Y. S. Guan, Y. Z. Chen, L. Z. Wu, C. H. Tung and Q. Z. Yang, *J. Am. Chem. Soc.*, 2012, **134**, 18928-18931.
3 J. Liu, Y. Liu, Q. Liu, C. Li, L. Sun and F. Li, *J. Am. Chem. Soc.*, 2011, **133**, 15276-15279.
4 M. Lan, J. Zhang, Y. S. Chui, P. Wang, X. Chen, C. S. Lee, H. L. Kwong and W. Zhang, *ACS Appl. Mater. Interfaces*, 2014, **6**, 21270-21278.
5 Y. Yan, H. Yu, Y. Zhang, K. Zhang, H. Zhu, T. Yu, H. Jiang and S. Wang, *ACS Appl. Mater. Interfaces*, 2015, **7**, 3547-3553.
6 A. Zhu, Q. Qu, X. Shao, B. Kong and Y. Tian, *Angew. Chem., Int. Ed.*, 2012, **51**, 7185-7189.
7 A. Burns, H. Ow and U. Wiesner, *Chem. Soc. Rev*, 2006, **35**, 1028-1042.
8 X. Cheng, Q. Li, J. Qin and Z. Li, *ACS Appl. Mater. Interfaces*, 2010, **2**, 1066-1072.
9 Y. Chen, C. Zhu, Z. Yang, J. Chen, Y. He, Y. Jiao, W. He, L. Qiu, J. Cen and Z. Guo, *Angew. Chem., Int. Ed.*, 2013, **52**, 1688-1691.
10 Z. X. Han, X. B. Zhang, Z. Li, Y. J. Gong, X. Y. Wu, Z. Jin, C. M. He, L. X. Jian, J. Zhang, G. L. Shen and R. Q. Yu, *Anal. Chem.*, 2010, **82**, 3108-3113.
11 Z. Liu, C. Zhang, W. He, Z. Yang, X. Gao and Z. Guo, *Chem. Commun.*, 2010, **46**, 6138-6140.

12 K. Zhang, H. Zhou, Q. Mei, S. Wang, G. Guan, R. Liu, J. Zhang and Z. Zhang, *J. Am. Chem. Soc.*, 2011, **133**, 8424-8427.
13 X. Yan, H. Li, Y. Li and X. Su, *Anal. Chim. Acta.*, 2014, **852**, 189-195.
14 Q. Mu, Y. Li, H. Xu, Y. Ma, W. Zhu and X. Zhong, *Talanta*, 2014, **119**, 564-571.
15 J. Yao, K. Zhang, H. Zhu, F. Ma, M. Sun, H. Yu, J. Sun and S. Wang, *Anal. Chem.*, 2013, **85**, 6461-6468.
16 L.-H. Jin and C.-S. Han, *Anal. Chem.*, 2014, **86**, 7209-7213.
17 L. Lu, G. Yang and Y. Xia, *Anal. Chem.*, 2014, **86**, 6188-6191.
18 K. Zhang, T. Yu, F. Liu, M. Sun, H. Yu, B. Liu, Z. Zhang, H. Jiang and S. Wang, *Anal. Chem.*, 2014, **86**, 11727-11733.
19 A. P. Alivisatos, *Science*, 1996, **271**, 933.
20 X. Michalet, F. Pinaud, L. Bentolila, J. Tsay, S. Doose, J. Li, G. Sundaresan, A. Wu, S. Gambhir and S. Weiss, *Science*, 2005, **307**, 538-544.
21 A. Guerrero-Martínez, J. Pérez-Juste and L. M. Liz-Marzán, *Adv. Mater.*, 2010, **22**, 1182-1195.
22 S. W. Bae, W. Tan and J. I. Hong, *Chem. Commun.*, 2012, **48**, 2270-2282.
23 X. Sun, B. Liu and Y. Xu, *Analyst*, 2012, **137**, 1125-1129.
24 H. Zhu, T. Yu, H. Xu, K. Zhang, H. Jiang, Z. Zhang, Z. Wang and S. Wang, *ACS Appl. Mater. Interfaces*, 2014, **6**, 21461-21467.
25 Y. Yan, J. Sun, K. Zhang, H. Zhu, H. Yu, M. Sun, D. Huang and S. Wang, *Anal. Chem.*, 2015, **87**, 2087-2093.
26 K. Zhang, L. Yang, H. Zhu, F. Ma, Z. Zhang and S. Wang, *Analyst*, 2014, **139**, 2379-2385.
27 X. Yan, H. Li, X. Han and X. Su, *Biosens. Bioelectron.*, 2015, **74**, 277-283.
28 Y. Q. Wang, T. Zhao, X. W. He, W. Y. Li and Y. K. Zhang, *Biosens. Bioelectron.*, 2014, **51**, 40-46.
29 J. Wang, M. Ma, R. Huang, L. Wang, A. Chen and J. Hu, *Anal. Methods*, 2015, **7**, 2295-2299.
30 A. M. Derfus, W. C. Chan and S. N. Bhatia, *Nano lett.*, 2004, **4**, 11-18.
31 R. Werlin, J. H. Priester, R. E. Mielke, S. Kramer, S. Jackson, P. K. Stoimenov, G. D. Stucky, G. N. Cherr, E. Orias and P. A. Holden, *Nat. Nanotechnol.*, 2011, **6**, 65-71.
32 L. Jing, Y. Li, K. Ding, R. Qiao, A. L. Rogach and M. Gao, *Nanotechnology*, 2011, **22**, 505104.
33 Y. Yang and M. Gao, *Adv. Mater.*, 2005, **17**, 2354-2357.
34 B. Liu, F. Zeng, G. Wu and S. Wu, *Analyst*, 2012, **137**, 3717-3724.
35 Y. Zhu, Z. Li, M. Chen, H. M. Cooper and Z. P. Xu, *J. Mater. Chem. B*, 2013, **1**, 2315.
36 W. Stober and A. Fink, *J. colloid Interface Sci.*, 1968, **26**, 62-69.
37 J. Wang, H. Han, X. Jiang, L. Huang, L. Chen and N. Li, *Anal. Chem.*, 2012, **84**, 4893-4899.
38 Y. Zhu, Z. Li, M. Chen, H. M. Cooper, G. Q. Lu and Z. P. Xu, *Chem. Mater.*, 2012, **24**, 421-423.
39 39. Y. Song, X. Cao, Y. Guo, P. Chen, Q. Zhao and G. Shen, *Chem. Mater.*, 2009, **21**, 68-77.
40 Y. Zhu, Z. Li, M. Chen, H. M. Cooper, G. Q. Lu and Z. P. Xu, *J. colloid Interface Sci.*, 2013, **390**, 3-10.
41 D. K. Yi, S. T. Selvan, S. S. Lee, G. C. Papaefthymiou, D. Kundaliya and J. Y. Ying, *J. Am. Chem. Soc.*, 2005, **127**, 4990-4991.
42 F. Gao, Q. Ye, P. Cui and L. Zhang, *J. Agric. Food Chem.*, 2012, **60**, 4550-4558.
43 N. Gaponik, D. V. Talapin, A. L. Rogach, K. Hoppe, E. V. Shevchenko, A. Kornowski, A. Eychmüller and H. Weller, *J. Phys. Chem. B*, 2002, **106**, 7177-7185.
44 B.-H. Jun, D. W. Hwang, H. S. Jung, J. Jang, H. Kim, H. Kang, T. Kang, S. Kyeong, H. Lee, D. H. Jeong, K. W. Kang, H. Youn, D. S. Lee and Y.-S. Lee, *Adv. Funct. Mater.*, 2012, **22**, 1843-1849.
45 H. Dong, F. Yan, H. Ji, D. K. Y. Wong and H. Ju, *Adv. Funct. Mater.*, 2010, **20**, 1173-1179.
46 H. Zhang, Z. Zhou, B. Yang and M. Gao, *J. Phys. Chem. B*, 2003, **107**, 8-13.
47 D. Knopp, D. Tang and R. Niessner, *Anal. Chim. Acta.*, 2009, **647**, 14-30.
48 E. Oh, M.-Y. Hong, D. Lee, S.-H. Nam, H. C. Yoon and H.-S. Kim, *J. Am. Chem. Soc.*, 2005, **127**, 3270-3271.
49 M. Li, S. K. Cushing, Q. Wang, X. Shi, L. A. Hornak, Z. Hong and N. Wu, *J. Phys. Chem. Lett.*, 2011, **2**, 2125-2129.
50 M. Li, Q. Wang, X. Shi, L. A. Hornak and N. Wu, *Anal. Chem.*, 2011, **83**, 7061-7065.
51 L. Wang, W. Zhao and W. Tan, *Nano Res.*, 2008, **1**, 99-115.
52 K. Saha, S. S. Agasti, C. Kim, X. Li and V. M. Rotello, *Chem. Rev.*, 2012, **112**, 2739-2779.

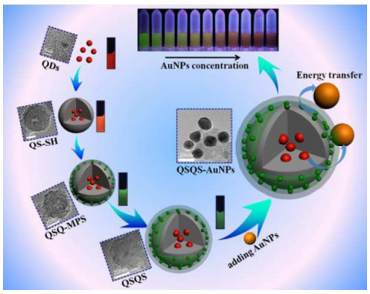

Highly stable and biocompatible $CdTe@SiO_2@CdTe@SiO_2$ dual-emission hierarchical hybrid nanostructure was synthesized and served as robust ratiometric fluorescent sensor.